Homogeneous vibrational dynamics and inhomogeneous broadening in glass-forming liquids: Infrared photon echo experiments from room temperature to 10 K

A. Tokmakoff[a] and M. D. Fayer
Department of Chemistry, Stanford University, Stanford, California 94305

(Received 23 December 1994; accepted 9 May 1995)

A study of the temperature dependence of the homogeneous linewidth and inhomogeneous broadening of a high-frequency vibrational transition of a polyatomic molecule in three molecular glass-forming liquids is presented. Picosecond infrared photon echo and pump–probe experiments were used to examine the dynamics that give rise to the vibrational line shape. The homogeneous vibrational linewidth of the asymmetric CO stretch of tungsten hexacarbonyl ($\sim$1980 cm^{-1}) was measured in 2-methylpentane, 2-methyltetrahydrofuran, and dibutylphthalate from 300 K, through the supercooled liquids and glass transitions, to 10 K. The temperature dependences of the homogeneous linewidths in the three glasses are all well described by a T^2 power law. The absorption linewidths for all glasses are seen to be massively inhomogeneously broadened at low temperature. In the room temperature liquids, while the vibrational line in 2-methylpentane is homogeneously broadened, the line in dibutylphthalate is still extensively inhomogeneously broadened. The contributions of vibrational pure dephasing, orientational diffusion, and population lifetime to the homogeneous line shape are examined in detail in the 2-methylpentane solvent. The complete temperature dependence of each of the contributions is determined. For this system, the vibrational line varies from inhomogeneously broadened in the glass and low temperature liquid to homogeneously broadened in the room temperature liquid. The homogeneous linewidth is dominated by the vibrational lifetime at low temperatures and by pure dephasing in the liquid. The orientational relaxation contribution to the line is significant at some temperatures but never dominant. Restricted orientational relaxation at temperatures below $\sim$120 K causes the homogeneous line shape to deviate from Lorentzian, while at higher temperatures the line shape is Lorentzian. © *1995 American Institute of Physics.*

I. INTRODUCTION

Vibrational line shapes in condensed phases contain the details of the interactions of a normal mode with its environment. These interactions include the important microscopic dynamics, intermolecular couplings, and time scales of solvent evolution that modulate the energy of a transition, in addition to essentially static structural perturbations. An infrared absorption spectrum or Raman spectrum gives frequency-domain information on the ensemble-averaged interactions that couple to the states involved in the transition.[1–3] Line shape analysis of vibrational transitions has long been recognized as a powerful tool for extracting information on molecular dynamics in condensed phases.[4,5] The difficulty with determining the microscopic dynamics from a spectrum arises because linear spectroscopic techniques have no method for separating the various contributions to the vibrational line shape. The IR absorption or Raman line shape represents a convolution of the various dynamic and static contributions to the observed line shape. In some cases, polarized Raman spectra can be used to separate orientational and vibrational dynamics from the line shape, yet as with all linear spectroscopies, contributions from inhomogeneous broadening cannot be eliminated.[6]

In order to completely understand a vibrational line shape, a series of experiments are required to characterize each of its static and dynamic components. These experiments can be effectively accomplished in the time domain, where well-defined techniques exist for measuring the various quantities. Nonlinear vibrational spectroscopy can be used to eliminate static inhomogeneous broadening from IR and Raman line shapes.[6] Techniques such as the infrared photon echo[7–9] and Raman echo[10–13] can determine the homogeneous vibrational line shape which contains the important microscopic dynamics when this line shape is masked by inhomogeneous broadening. Yet nonlinear time-domain techniques alone cannot separate the various dynamic contributions to the homogeneous vibrational line shape. Traditional time-domain experiments, such as transient absorption pump–probe experiments, are needed to observe population dynamics such as the vibrational lifetime and orientational relaxation. To further characterize the long time-scale dynamics of spectral diffusion within the line, additional experiments, such as stimulated photon echoes[14] or transient hole burning,[15] are required.

In this paper we present a detailed study of the temperature dependence of the infrared line shape of a high-frequency vibrational transition of a solute in three molecular glass-forming liquids between 10 and 300 K using picosecond infrared photon echo and pump–probe experiments. These experiments are the first to follow the evolution with temperature of the dynamics that comprise the vibrational

[a]Present address: Physik Department E11, Technische Universität München, D-85748 Garching, Germany.

 0021-9606/95/103(8)/2810/17/$6.00

line shape in amorphous condensed phases and to quantify the degree of inhomogeneous broadening for these systems. The dynamics cover temperature regions from the low temperature glass, through the glass transition and supercooled liquid, to the room temperature liquid. The results are of significance for the understanding of various vibrational dynamic phenomena in condensed phases, and have relevance to the study of fast dynamics in the passage through the glass transition. These results also form a basis for comparison with a number of theories of dephasing in liquids,[4,16–18] and in glasses.[19,20]

Temperature-dependent studies of condensed matter vibrational dynamics are of importance for understanding the coupling of vibrational modes with the external degrees of freedom of the solvent. The population and density of states of low frequency modes of a solvent and the coupling of these modes to internal molecular vibrations dictate the vibrational dynamics. Despite their importance in a wide variety of fields of chemistry, biology, and physics, relatively little is known about the temperature-dependent dynamics of molecular vibrations in polyatomic liquids and glasses. Although a great deal of work has been done using line shape analysis of vibrational transitions, there have only been a few studies that unambiguously eliminated inhomogeneous broadening and examined the temperature dependence of the homogeneous dynamics. Raman echo measurements of dephasing of C–H stretching modes in ethanol liquid and glass[13] have demonstrated that the line is homogeneously broadened at all temperatures between 10 and 300 K. It has been proposed that in this system fast intramolecular vibrational energy redistribution determines the linewidth. Measurements of line narrowed vibrational line shapes in glasses and crystals have been performed with persistent infrared hole burning.[21–24] While hole burning and Raman echoes are vibrational line narrowing techniques, in general they cannot distinguish among the contributions to the homogeneous vibrational line shape from lifetime, rotation, and pure dephasing. In addition, hole burning cannot discriminate between homogeneous dephasing and additional line broadening contributions from longer time scale spectral diffusion.[14] Many of these problems are being overcome with time-resolved resonant infrared experiments. Temperature-dependent picosecond infrared studies of discrete vibrations in liquids and glasses have observed homogeneous vibrational dephasing with photon echoes[7–9] and vibrational population lifetimes with pump–probe experiments[7,15,25,26] and picosecond transient hole burning.[27]

Below we present the temperature-dependent vibrational dynamics of the triply degenerate T_{1u} CO stretching mode of tungsten hexacarbonyl [$W(CO)_6$] in the molecular glass-forming liquids 2-methyltetrahydrofuran (2-MTHF), 2-methylpentane (2-MP), and dibutylphthalate (DBP). Two aspects of the vibrational line shape in these systems are discussed in detail. Initially, we compare the behavior of the homogeneous linewidths in the glasses and the transition to the room temperature liquids for the three glasses, using ps IR photon echo experiments. The temperature dependence of the vibrational dephasing and the degree of inhomogeneity as the liquids approach room temperature are described. The temperature dependence of the homogeneous vibrational linewidth in the three glassy solvents is T^2 within experimental error, but the behavior is distinct in each of the liquids. While in 2-MP the vibrational line is homogeneously broadened at room temperature, the line in DBP is massively inhomogeneously broadened in the room temperature liquid.

Following the comparison of the temperature-dependent dephasing in the three solvents, one of the systems, $W(CO)_6$ in 2-MP, is analyzed in greater detail. The contributions to the vibrational line shape from different dynamic processes are delineated by combining the results of photon echo measurements of the homogeneous line shape[8] with pump–probe measurements of the lifetime and reorientational dynamics.[15] This combination of measurements allows the decomposition of the total homogeneous vibrational line shape into the individual components of pure-dephasing (T_2^*), population relaxation (T_1), and orientational relaxation. The results demonstrate that each of these can contribute significantly, but to varying degrees at different temperatures.

$W(CO)_6$ was chosen as a well-understood vibrational chromophore to use as a dilute probe of intermolecular solvent interactions while discriminating against solute–solute effects. It is soluble in a wide variety of solvents, and it is stable under normal experimental conditions. The CO stretch of $W(CO)_6$ has a particularly strong transition dipole moment in the infrared, allowing very dilute solutions to be probed and strong photon echo signals to be observed. The absorption linewidth for this transition is very narrow, permitting dynamics to be characterized with picosecond pulses. Also, several aspects of the dynamics of this probe molecule have previously been characterized in a number of liquids and glasses.[7,8,9,15,25,28,29] The degenerate nature of the transition studied makes the analysis of the orientational relaxation more involved, yet ultimately contributes more information on the temperature-dependent dynamics.

The paper is divided as follows. In Sec. II, the dipole correlation function formalism that relates the microscopic dynamics of the vibrational dipole to the infrared line shape and the infrared photon echo experiment is discussed. This material is presented because the influence of orientational relaxation and restricted orientational relaxation on the photon echo observable has not been discussed previously. The results are given in the text while the full treatments are reserved for the appendices. The experimental procedures and results are described in Secs. III and IV. The discussion is divided into two sections. Section V A is a comparison of the temperature dependences of vibrational dephasing in the three glasses. Section V B is a detailed discussion of the liquid 2-MP, in which the temperature dependence of all dynamic contributions to the vibrational line shape are delineated. A summary and concluding remarks are given in Sec. VI.

II. THEORETICAL BACKGROUND

A. Correlation function description of the vibrational line shape

For a dilute solution of a vibrational chromophore, the homogeneous vibrational linewidth, Γ, generally has contri-

butions from the rate of population relaxation (lifetime), $1/T_1$, the rate of pure dephasing, $1/T_2^*$, and the rate of orientational relaxation, Γ_{or}. T_1 processes are caused by the anharmonic coupling of the vibrational mode to the bath, which includes other vibrational modes of the solute and the solvent and the low frequency continuum of intermolecular solvent modes or phonons.[17,25,30,31] Population relaxation is the only dynamic process that can contribute to the vibrational linewidth in the limit that $T \rightarrow 0$ K.[31,32] Pure dephasing describes the adiabatic modulation of the vibrational energy levels of a transition caused by thermal fluctuations of its environment.[18,33] Measurement of this quantity provides detailed insight into the fast dynamics of the system. Although generally equated with physical rotation of the dipole, orientational relaxation is defined as any process that causes the loss of angular correlation of an ensemble of dipoles. For the T_{1u} mode of $W(CO)_6$ studied here, orientational relaxation occurs through the time evolution of the coefficients of the three states in the superposition state created by the initial excitation of the triply degenerate T_{1u} mode. Both pure dephasing and orientational relaxation will vanish in the limit that $T \rightarrow 0$ K, since they are thermally induced processes.

The infrared absorption line shape is related to these microscopic dynamics through the Fourier transform of the two-time transition dipole correlation function[1,2,3,33]

$$I(\omega) = (2\pi)^{-1} \int_{-\infty}^{+\infty} dt e^{i\omega t} \langle \boldsymbol{\mu}(t) \cdot \boldsymbol{\mu}^*(0) \rangle. \tag{1}$$

The infrared absorption spectrum gives dynamic information on $\langle P_1(\mu(t)\mu^*(0)) \rangle$, where P_l is the Legendre polynomial of order l. A similar equation is valid for Raman or light scattering experiments where the time correlation function of the molecular polarizability is considered; these experiments give information in the form of P_2.[34]

If the vibrational and rotational motions are decoupled, then the dipole correlation function can be factored

$$\langle \boldsymbol{\mu}(t) \cdot \boldsymbol{\mu}^*(0) \rangle = \langle \mu(t)\mu^*(0) \rangle \langle \hat{\mu}(t) \cdot \hat{\mu}(0) \rangle. \tag{2}$$

The first term in Eq. (2) describes only the time dependence of the nuclear motions and is often written as[35]

$$\langle \mu(t)\mu^*(0) \rangle = |\mu|^2 \left\langle \exp\left[-i \int_0^t dt' \Delta(t') \right] \right\rangle. \tag{3}$$

Here Δ describes the variations in the transition energies for the ensemble of vibration transition dipoles and includes any inhomogeneous broadening.[14] The second term in Eq. (2) is the ensemble averaged correlation function for unit vectors along the dipole direction and describes the orientational motion of the dipole.

In the Markovian limit, in which these quantities are described by independent exponentially relaxing dipole correlation functions, the total dipole correlation function described by Eq. (2) decays exponentially at a rate of $1/T_2$, the dephasing time. Equation (1) gives a Lorentzian line shape, and contributions to the full line width at half-maximum (FWHM) are additive

$$\Gamma = 1/\pi T_2 = 1/\pi T_2^* + 1/2\pi T_1 + \Gamma_{or}. \tag{4}$$

The orientational contribution to the infrared line shape due to isotropic rotational diffusion of the dipole is determined by $\langle P_1(\hat{\mu}(t) \cdot \hat{\mu}(0)) \rangle$ and, as shown in Appendix A, is given by

$$\Gamma_{or} = 2D_{or}/\pi, \tag{5}$$

where D_{or} is the orientational diffusion constant. This form arises from the general relation of the time-dependent decay of $\langle P_l(\hat{\mu}(t) \cdot \hat{\mu}(0)) \rangle$ to the expansion coefficients of the Green's function solution to the orientational diffusion equation[36,37]

$$c_l^m(t) = e^{-l(l+1)D_{or}t}. \tag{6}$$

Equation (4) allows the contribution of pure dephasing to the vibrational line shape to be determined from a knowledge of the homogeneous linewidth, the vibrational lifetime, and the orientational diffusion constant.

B. The infrared photon echo experiment

The infrared photon echo[7–9] is a time-domain nonlinear technique that allows inhomogeneity to be removed from the vibrational line shape. It is the infrared vibrational equivalent of photon echoes conducted on electronic states with visible pulses and spin echoes in magnetic resonance. Two short IR pulses, tuned to the molecular vibration of interest, are crossed in the sample. The first pulse creates a coherent state that begins to dephase due to both its interactions with the dynamic environment and the static inhomogeneity. A second pulse, delayed by time τ, initiates rephasing of the inhomogeneous contributions to the vibrational transition; however, homogeneous dephasing is irreversible. This rephasing results in a macroscopic polarization that is observed as an echo pulse in a unique direction at time 2τ. The integrated intensity of the echo pulse is measured as a function of τ, and its decay time with τ is proportional to the homogeneous dephasing time of the vibrational transition. The rephasing of the inhomogeneous broadening eliminates its contribution to the signal.

The infrared absorption line shape, including any inhomogeneity, is governed by a two-time correlation function. The two-pulse photon echo, and other line narrowing techniques such as the stimulated photon echo and hole burning, eliminate the inhomogeneous contribution to the line shape and are described by four-time correlation functions[6] of the form

$$C = \langle \boldsymbol{\mu}^*(t_3 + t_2 + t_1) \cdot \boldsymbol{\mu}(t_2 + t_1) \cdot \boldsymbol{\mu}(t_1) \cdot \boldsymbol{\mu}^*(0) \rangle, \tag{7}$$

where t_1, t_2, and t_3 refer to three consecutive time intervals. We have written this form[38] of the correlation function for direct comparison to Eq. (1). Just as the quantum mechanical correlation function in Eq. (1) can also be written in terms of the anticommutator $\langle \{\boldsymbol{\mu}(t), \boldsymbol{\mu}(0)\}/2 \rangle$, the correlation function in Eq. (7) is normally written as a trace over three nested commutators of a dipole operator with the density matrix using the Heisenberg representation.[39] This form yields four correlation functions (and their complex conjugate) in the form of Eq. (7) that contribute to the observed signal, two of which describe photon echo experiments.[40,41] The two-pulse photon echo is a third-order nonlinear experiment that uses

three input fields E_i resonant with a vibrational transition to generate an output echo signal described by $C(t_3,t_2,t_1)$. The first field interaction is during the first pulse, and the second and third interactions are with the second pulse. For a pulse separation τ, the experiment is described by correlation functions of the form $\langle \boldsymbol{\mu}^*(2\tau)\cdot\boldsymbol{\mu}(\tau)\cdot\boldsymbol{\mu}(\tau)\cdot\boldsymbol{\mu}^*(0)\rangle$.

As with the two-time correlation function, the assumption that vibrational and rotational degrees of freedom are independent allows the four-time correlation function C to be separated as $C=C_V C_{\mathrm{OR}}$. The vibrational contribution to the four-time correlation function C_V is given by[6,39,42]

$$C_V(t_3,t_2,t_1)=|\mu|^4\left\langle \exp\left[i\int_{t_1+t_2}^{t_1+t_2+t_3} dt'\,\Delta(t') - i\int_0^{t_1} dt'\,\Delta(t')\right]\right\rangle. \tag{8}$$

Unlike Eq. (3), Eq. (8) allows for time reversal processes to remove inhomogeneity. The contribution of orientational relaxation to the correlation function C_{OR} can be written as

$$C_{\mathrm{OR}}(t_3,t_2,t_1)=\langle \hat{\mu}(t_3+t_2+t_1)\cdot\hat{\mu}(t_2+t_1)\cdot\hat{\mu}(t_1)\cdot\hat{\mu}(0)\rangle, \tag{9}$$

which is the ensemble averaged four-time correlation function for unit vectors along the transition dipole direction. C_{OR} can be treated as a classical probability average when the orientational relaxation is diffusive.

The description of the third-order nonlinear polarization that governs infrared photon echo experiments in terms of the dynamics of lifetime, pure dephasing, and orientational diffusion is discussed in Appendix A. For the case that the relaxation processes that contribute to the line shape are separable, the photon echo signal with delta function pulses decays exponentially as

$$I(\tau)/I(0)=\exp[-4\tau(1/T_2^*+1/2T_1+2D_{\mathrm{OR}})] \tag{10a}$$

$$=\exp[-4\tau/T_2]. \tag{10b}$$

The signal decays at a rate four times faster than the decay of the homogeneous dipole correlation function. The decay of the photon echo in this limit can be written as proportional to $|\langle \boldsymbol{\mu}(\tau)\cdot\boldsymbol{\mu}^*(0)\rangle|^4$, and thus gives the homogeneous vibrational line shape through Eq. (1). It is important to note that due to the separability of the rotational and vibrational degrees of freedom and the Markovian form of the correlation function decay, the four-time correlation function can be written as the product of two-time correlation functions.

III. EXPERIMENTAL PROCEDURES

Vibrational photon echoes were performed with infrared pulses at approximately 5 μm generated by the Stanford superconducting-accelerator-pumped free electron laser (FEL). The FEL generates Gaussian pulses that are transform limited with pulse length (bandwidth) variable from about 0.7 to 2.0 ps. The wavelength is tunable in 0.01 μm increments; active frequency stabilization allows wavelength

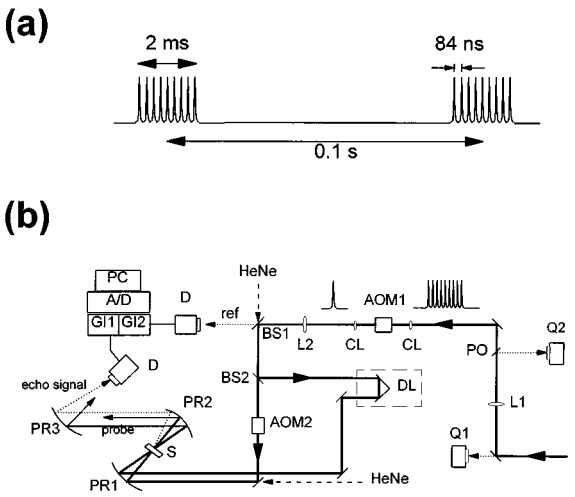

FIG. 1. (a) FEL pulse train structure. The macropulse repetition rate is 10 Hz, with a 2 ms envelope. The micropulse repetition rate is 12 MHz within the macropulse. (b) FEL experimental apparatus. Pulse selection is accomplished with AOM1, while AOM2 is used for chopping of pulse 2. AOM, acousto-optic modulator; A/D, analog-to-digital converter; BS, ZnSe beam splitter; CL, cylindrical lens; D, detector; DL, optical delay line; GI, gated integrator; L, lens; PC, personal computer; PO, pick-off; PR, off-axis parabolic reflector; Q, position sensitive detector; S, sample.

drifts to be limited to $<0.01\%$, or <0.2 cm^{-1}. The pulse length and spectrum are monitored continuously with an autocorrelator and grating monochromator.

Acquisition of data requires manipulation of the unusual FEL pulse train shown in Fig. 1(a). The FEL emits a 2 ms macropulse at a 10 Hz repetition rate. Each macropulse consists of the ps micropulses at a repetition rate of 11.8 MHz (84 ns). The micropulse energy at the input to experimental optics is $\sim$0.5 μJ, and the corresponding energy in the full FEL beam is 120 mW. In vibrational experiments, virtually all power absorbed by the sample is deposited as heat. To avoid sample heating problems, micropulses are selected out of the macropulse at a reduced frequency.

The experimental apparatus is shown in Fig. 1(b). The infrared beam enters the experimental area roughly collimated with a 16 mm diam. Beam pointing stability is monitored with two position sensitive detectors. A 1:6$\times$telescope (L1 & L2) reduces the beam size. At the focus of the telescope is a Ge acousto-optic modulator (AOM) for pulse selection, within a 1:1 cylindrical telescope using CaF_2 lenses. Micropulses are selected out of each macropulse at a repetition rate of 50 kHz by the AOM single pulse selector. The cylindrical telescope makes the AOM rise time less than the interpulse separation. This pulse selection yields an effective experimental repetition rate of 1 kHz, and an average power <0.5 mW. A ZnSe beam splitter allows 1% of the IR beam to be directed into a HgCdTe reference detector. The reference detector was used for shot intensity windowing; all data from pulses with intensities outside of a 10% window were discarded.

The two pulses for photon echo or pump–probe experiments were obtained with a 10% ZnSe beam splitter. The 10% beam (first pulse in echo sequence and probe pulse) is sent through a computer-controlled stepper motor delay line.

The remaining portion (second echo pulse or pump pulse) is chopped at 25 kHz by a second Ge AOM. A HeNe beam is made collinear with each IR beam for alignment purposes. The two pulses were focused in the sample to 220 μm diameter using an off-axis parabolic reflector, for achromatic focusing of the IR and HeNe. The beams and echo signal were recollimated with a second parabolic reflector, and focused into a HgCdTe signal detector with a third parabolic reflector. By selecting the desired beam with an iris between the second and third parabolic reflectors, either the photon echo or pump–probe signal could be observed. The photon echo signal and an intensity reference signal were sampled by two gated integrators and digitized for collection by computer.

Careful studies of power dependence and repetition rate dependence of the data were performed. It was determined that there were no heating or other unwanted effects when data were taken with pulse energies of ~15 nJ for the first pulse, ~80 nJ for the second pulse, and the effective repetition rate of 1 kHz (50 kHz during each macropulse).

Vibrational photon echo and pump–probe data were taken on the triply degenerate T_{1u} asymmetric CO stretching mode of $W(CO)_6$. Solutions of $W(CO)_6$ in the glass-forming liquids were made to give a peak optical density of 0.8 with thin path length. Concentrations varied from 0.6 mM with a 200 μm path length for 2-MP, to 4 mM with a 400 μm path length for DBP. (The difference arises because of the much broader inhomogeneous line found in DBP, which is discussed below.) These solutions correspond to mole fractions of $\leqslant 10^{-4}$, and are dilute enough to eliminate Förster resonant energy transfer.[28] 2-MP (>99.9%), DBP (>99%), and $W(CO)_6$ (99%) were purchased and used without further purification. 2-MTHF (99%) was distilled in order to remove peroxide inhibitors added by the vendor. The temperature of the sample was controlled to ± 0.2 K using a closed-cycled He refrigerator. After equilibration, the temperature gradient across the sample never exceeded ± 0.2 K.

The temperature dependences of the vibrational absorption spectra were characterized by infrared absorption spectra. Fourier transform infrared spectra of the 2-MTHF and 2-MP samples were taken with 0.25 cm^{-1} resolution using the same closed cycled helium refrigerator. Spectra on the DBP solution were taken with 2 cm^{-1} resolution using a variable temperature liquid nitrogen cryostat.

IV. RESULTS

The results of temperature-dependent photon echo experiments on the T_{1u} mode of $W(CO)_6$ in the three glass-forming liquids are shown in Fig. 2. Examples of the actual echo decay data have been shown elsewhere.[7–9] The homogeneous linewidth, $\Gamma = 1/\pi T_2$, is shown, derived from fits assuming that the photon echo signal decays exponentially as Eq. (10b). Data on 2-MTHF were taken from 10 up to 120 K, at which point the decay rate exceeded the instrument response. This data, although very similar, supersedes an earlier report on this liquid.[7] Echo data in the other liquids were observable up to room temperature. A preliminary description of the data for 2-MP has been given previously.[8] The data in DBP, taken with 0.7 ps pulses, has been discussed recently up to 150 K.[9] At temperatures above 150 K, rapid damping of additional decay processes from higher vibrational levels gave rise to the large error bars in the Fig. 2.

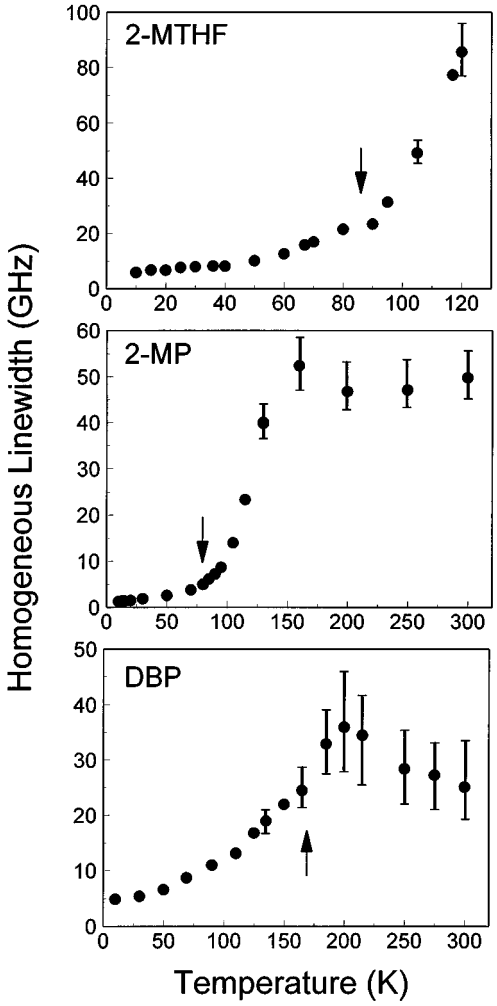

FIG. 2. Temperature dependence of the homogeneous linewidths of the T_{1u} CO stretching mode of $W(CO)_6$ in 2-MTHF, 2-MP, and DBP, determined from infrared photon echo experiments using Eq. (10b), i.e., the data decays exponentially at four times the homogeneous dephasing rate. Arrows mark the glass transition temperature. Note the different temperature and linewidth scales.

The temperature dependence of the homogeneous linewidth increases monotonically in the glass. Above the glass transition temperature, the linewidth in 2-MTHF ($T_g = 86$ K) and 2-MP ($T_g = 80$ K) rises rapidly in a manner that appears thermally activated. In 2-MP, the rapid increase in dephasing rate slows above 130 K and becomes temperature independent. In DBP ($T_g = 169$ K), the linewidth appears to decrease with temperature above 200 K although the error bars are large enough that it is possible that the temperature dependence is essentially flat.

Pump–probe measurements of the population dynamics in 2-MP and 2-MTHF taken with parallel pump and probe polarizations are shown in Fig. 3. A detailed analysis of the population dynamics and their temperature dependences for the 2-MP data are given in Ref. 15. The interpretation is identical for 2-MTHF. The data at all temperatures are biex-

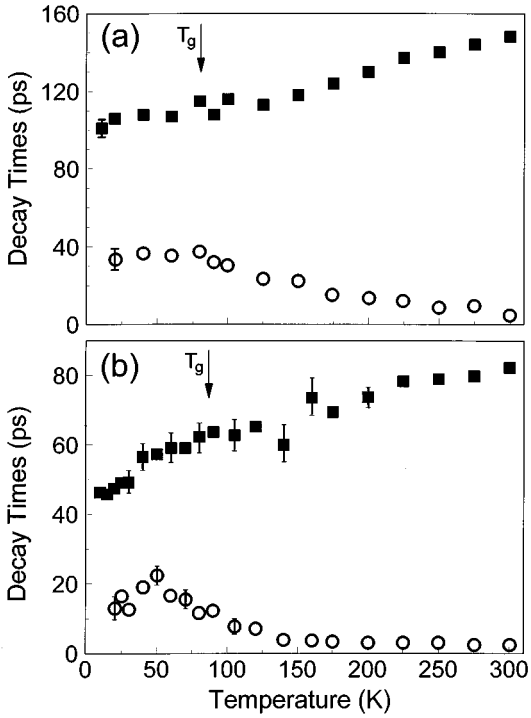

FIG. 3. Temperature-dependent population relaxation dynamics of the T_{1u} of $W(CO)_6$ in (a) 2-MP and (b) 2-MTHF. Each set of data shows the two decay components of the biexponential data from parallel-polarized pump–probe experiments. A detailed analysis of the dynamics and their temperature dependences for 2-MP are given in Ref. 15. The interpretation is identical for 2-MTHF. The solid squares represent the population lifetime T_1. The open circles are a fast component that is due to orientational relaxation of the chromophore.

ponential. The decay times of the two decay components are given in Fig. 3. The long decay component is due to vibrational population relaxation (lifetime), and decays with an exponential decay time of T_1. Both liquids have a counterintuitive temperature dependence, with the rate of relaxation decreasing as the temperature increases. This phenomenon has recently been observed in crystallizing and glass-forming liquids.[15,25] The fast component in the pump–probe data is due to orientational relaxation of the chromophore, and decays exponentially at a rate of $(6D_{or}+1/T_1)$. With magic angle probing to eliminate orientational relaxation effects, the fast component vanished from the decay, leaving only the long component. The amplitudes of the decay components are consistent with complete orientational relaxation above ~120 K and restricted relaxation at lower temperatures. The pump–probe data on 2-MTHF supersede the preliminary data reported on this system.[7]

The absorption linewidths for the T_{1u} mode of $W(CO)_6$ in the three glass-forming liquids are shown in Fig. 4. The absorption linewidth in DBP is 26 cm^{-1} and is temperature independent. In 2-MTHF, the linewidth varies somewhat from 16 cm^{-1} at room temperature to 19 cm^{-1} at 10 K. The spectrum in 2-MP shows the most change with temperature. In the glass, the absorption line is ~10 cm^{-1} wide. Above the glass transition, the line narrows rapidly to a minimum linewidth of 3.2 cm^{-1} at 250 K and broadens slightly at higher temperatures. The absorption linewidths for all solutions are wider than the homogeneous linewidths measured with the echo experiments at all temperatures with the exception of 2-MP above 200 K. As will be discussed below, proper interpretation of the echo decays above 200 K demonstrates that the absorption line in 2-MP is homogeneously broadened.

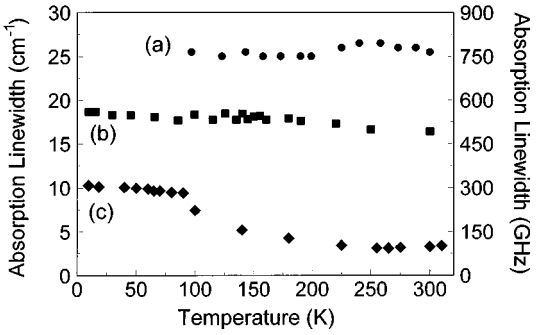

FIG. 4. Temperature dependence of the infrared absorption linewidth of the T_{1u}CO stretching mode of $W(CO)_6$ in (a) DBP, (b) 2-MTHF, and (c) 2-MP.

The temperature dependences of the homogeneous vibrational linewidths in the three glasses are compared using a reduced variable plot in Fig. 5. Although the absolute linewidths for each system may vary, this is a reflection of the strength of coupling of the transition dipole to the bath, and can be removed by normalization to the linewidth at the glass transition temperature. Likewise, using a reduced temperature T/T_g allows thermodynamic variables that contribute to determining the glass transition to be normalized. Such normalization allows comparison of the functional form of the temperature dependences, independent of differences in T_g and coupling strengths. Figure 5 shows that the temperature dependences of the homogeneous linewidths are identical in the three glasses and are well described by a power law of the form

$$\Gamma(T)=\Gamma_0+AT^{\alpha}. \tag{11}$$

The offset at 0 K, Γ_0, represents the linewidth due to the low temperature vibrational lifetime. A fit to Eq. (11) for all tem-

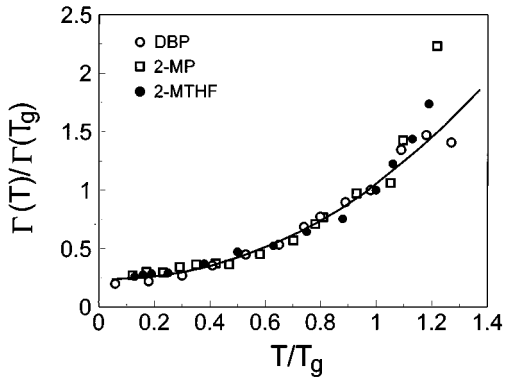

FIG. 5. Comparison of the homogeneous infrared linewidth in three organic glasses. The homogeneous linewidth normalized to the linewidth at the glass transition temperature to remove the coupling strength is plotted against the reduced temperature. The temperature dependence follows a power law with exponent $\alpha=2.1\pm0.2$.

TABLE I. Fit parameters for all glasses to Eq. (11).

		Power law fit to T_g $1/\pi T_2$			Power law fit to T_g $1/\pi T_2 - 1/2\pi T_1$	
Liquid	T_g (K)	log(A) (GHz)	α	T_2(0 K) (ps)	log(A) (GHz)	α
2-MP	79.5	-3.2 ± 0.4	2.0 ± 0.3	124 ± 2	-2.5 ± 0.3	2.2 ± 0.2
2-MTHF	86	-3.2 ± 0.4	2.3 ± 0.3	26 ± 2	-2.9 ± 0.3	1.9 ± 0.2
DBP	169	-3.3 ± 0.3	2.0 ± 0.1	33 ± 2	⋯	⋯
All liquids (Fig. 5)		$0.82\pm$ 0.03	2.1 ± 0.1	$(0.24\pm0.02)\times\Gamma(T_g)$	⋯	⋯

peratures below the glass transition is shown in Fig. 5, and yields an exponent of $\alpha=2.1\pm0.2$ and $\Gamma_0/\Gamma(T_g)=0.24\pm0.02$. At temperatures above $\sim 1.2T_g$, the linewidths of the three liquids diverge from one another. All of the liquids were individually fit to Eq. (11). The results are summarized in Table I, and demonstrate that the temperature dependence is well described by a power law of the form T^2.

Because of its high glass transition temperature, DBP allows the largest temperature range over which to observe the power law. The data are presented in two ways in Fig. 6. The solid circles are the data and the line through them is a fit to Eq. (11). To show more clearly the power law temperature dependence, the open circles are the data with the low temperature linewidth, Γ_0 [corresponding to a vibrational lifetime, $T_1(0\text{ K})=33$ ps] subtracted out. The line through the data is T^2. It can be seen that the power law describes the data essentially perfectly over a change of linewidth of $\sim$500 from 10 to 200 K. This temperature dependence is similar to that observed for infrared vibrational transitions in inorganic glasses with infrared hole burning.[22]

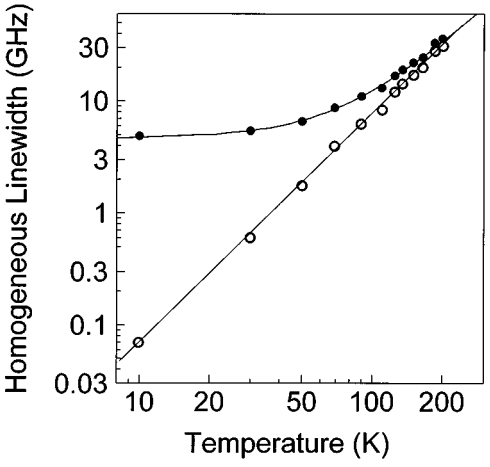

FIG. 6. Homogeneous linewidth of the T_{1u} mode of $W(CO)_6$ in DBP between 10 and 200 K. The homogeneous linewidth is shown in solid circles, and the corresponding data with the low temperature lifetime of $T_1(0\text{ K})=33$ ps removed are shown with open circles. The open circle data fit a power law of $\alpha=2.0\pm0.1$.

V. DISCUSSION

A. Comparison of vibrational dephasing in 2-MP, 2-MTHF, and DBP

1. Temperature dependence of dephasing in the glasses

The dynamics of optical dephasing in glasses[19] are generally interpreted within the model of two-level systems, initially proposed to describe their anomalous low temperature heat capacities.[43,44] In this model, pure dephasing dynamics are described in terms of phonon-induced tunneling between two structural potential wells. Above the Debye frequency of the glass, a power law of T^2 is theoretically predicted for dephasing due to two-phonon (Raman) scattering processes between potential wells.[19] Huber has pointed out that in glasses, this temperature dependence is expected above an effective Debye temperature, which can often be two to ten times lower than the true Debye temperature.[45] The $\alpha\approx2$ temperature dependence is almost universally seen for the high temperature dephasing of electronic transitions in a variety of glasses.[19] The temperature dependencies of vibrational linewidths using infrared hole burning have been observed to have similar temperature dependencies between 10 and 60 K. These include $\alpha=2.3$ for N–D stretches in mixed ammonium salts,[23] $\alpha=2.2$ and 2.0 for S–H and CO_2 defects in chalcogenide glasses,[22] and $\alpha=2.0$ for CN^- defects in CsCl crystals.[24] The same temperature dependence, $\alpha=2.08$, is seen for ReO_4^- impurity vibrations in alkali halide crystals.[20] Hole burning measures a linewidth with contributions from both homogeneous broadening and spectral diffusion.

Figure 5 demonstrates that the underlying temperature dependence of the vibrational homogeneous dephasing measured with the photon echoes is, in fact, identical in the three glasses studied here, and is described by a power law T^2. The results presented here are the first to examine the temperature dependence of vibrational dephasing in organic glasses. The observation of the T^2 dependence suggests that these glasses are in the high temperature limit above 10 K and that the temperature dependence of vibrational pure dephasing may be universal in all high temperature glasses. This would be consistent with dephasing caused by Raman (two quantum) phonon scattering.

Fits to Eq. (11) assume that the vibrational lifetime is

constant with temperature. However, T_1 can vary by ~50% over the temperature range. This variation of T_1 with temperature is relatively small compared to the power law temperature dependence. Equation (11) was fit to the 2-MP and 2-MTHF data after using the lifetime data of Fig. 3 to subtract out the temperature-dependent lifetime contribution to the linewidth according to Eq. (10). The parameters obtained from these fits, given in Table I, are slightly different but remain within the error bars of the original fit.

2. Temperature dependence above the glass transition

The temperature dependences of the rate of dephasing in 2-MP and 2-MTHF (Fig. 2) both show a gradual increase with temperature until shortly after the glass transition, at which point a rapid increase in dephasing is observed. Coincidentally, the glass transition temperatures for 2-MP (T_g=80 K) and 2-MTHF (T_g=86 K) are very similar. Thus, the rapid increase in dephasing can be explained by two possible phenomena: either by the emergence of additional solvent dynamics above the glass transition, or by thermally activated dephasing through coupling to a low frequency intramolecular mode of $W(CO)_6$. If one of the low frequency modes of $W(CO)_6$ is quadratically coupled to the T_{1u} mode, thermal population of this low frequency mode would result in thermally activated dephasing of the T_{1u} mode. For this mechanism, the break in the functional form of the temperature dependence would be independent of T_g. The temperature dependence of the T_{1u} vibrational linewidth in DBP shows no dramatic change near 90 K, demonstrating that such a mechanism is not the cause of the rapid increase in dephasing rates near 90 K in the other glasses. Rather, since the mechanism is dependent on the solvent, the dephasing is dictated by the particular temperature-dependent dynamics of the solvent.

At temperatures above the glass transition, the normalized linewidths in the three liquids diverge from each other, indicating the emergence of distinct relaxation processes in the various liquids. However, the temperature dependences observed in the glasses do not deviate from each other until $T/T_g>1.15$. In 2-MTHF and 2-MP, the rate of homogeneous dephasing increases rapidly above the glass transition temperature, in a manner that appears thermally activated. The temperature dependences for the two liquids are in fact very similar. Apart from coupling strength they are identical until ~130 K. At this temperature, the rate of increase of the dephasing in 2-MP slows as it approaches its high temperature behavior. The temperature dependence observed for DBP also deviates from the universal behavior observed in the glassy state for $T/T_g>1.15$, i.e., 30 degrees above the glass transition temperature.

The observation of a temperature for crossover between short time- and long time-scale structural relaxation processes in supercooled liquids is predicted by mode-coupling theory to occur slightly above the glass transition temperature.[46] This crossover temperature has been observed in many organic liquids to be $T_c=1.18T_g$.[47] T_c is regarded as the temperature below which relaxation processes bifurcate into two branches, α relaxations and β relaxations. α processes are longer time-scale structural evolution of a supercooled liquid which appear to freeze out on the relevant experimental time scale at the glass transition. β processes involve high frequency, more or less localized, molecular motions. The α relaxation processes are described by transport processes that can be related to the viscosity, translational and rotational diffusion, and dielectric relaxation. β relaxation processes are interpreted in terms of microscopic molecular fluctuations that exist at temperatures above and below the glass transition.[47] If β processes are coupled to the vibrational transition, they can contribute to the homogeneous vibrational dephasing. Although a change occurs in the temperature dependence of the vibrational dephasing at $\sim T_c$ above the glass transition, this may be a coincidence, not related to the bifurcation point. The onset of α relaxations have been reported near the glass transition using neutron scattering[48] and light scattering[49] experiments. The infrared photon echo is sensitive to fast dephasing dynamics (perhaps β relaxations) while it should be insensitive to slower structural processes, such as α relaxations near T_c. However, there is clearly a change in the dephasing dynamics in the range of temperatures around T_c. It is possible that the merging of the two relaxation branches at T_c modifies the coupling to the intramolecular vibration of the high frequency part of the fluctuation spectrum. The additional coupling might contribute substantially to the dephasing.

In contrast to the solvents 2-MP and 2-MTHF, there is no rapid increase in the homogeneous linewidth above the glass transition temperature in DBP. This observation shows that the temperature dependence is sensitive to the individual dynamics of the solvent. The differences in the dephasing data in the three solvents above T_g suggest that the rates of dephasing cannot be related to the solvent viscosity, even though the changes in the rates of dephasing are clearly due to the onset of additional relaxation processes above T_g. The additional processes may be new or involve dynamics that were too slow to cause dephasing below T_g. A fragility plot[50] of the viscosities of the three liquids[51–53] shows they superimpose. The temperature dependence of the viscosities, and thus the ability to assume structural configurations over longer time scales, is virtually identical for the three liquids. Thus differences in the temperature dependence of the dephasing in the three solvents at temperatures greater than $T/T_g=1.15$ cannot be ascribed to differences in the solvent fragilities.

In 2-MTHF and in 2-MP below 150 K, the echo decays yield a homogeneous linewidth that is much narrower than the width of the absorption spectrum. These results demonstrate that the vibrational lines of these system are inhomogeneously broadened in the glass and supercooled liquid. As shown below, in 2-MP the $W(CO)_6$ T_{1u} line becomes homogeneously broadened at room temperature. However, in DBP the line is clearly inhomogeneous at all temperatures. The homogeneous linewidth at 300 K is ~1 cm^{-1}, while the absorption spectrum linewidth is 26 cm^{-1}. This is the first conclusive evidence for intrinsic inhomogeneous broadening of a vibrational line in a room temperature liquid. Previously, measurements of room temperature homogeneous vibrational dephasing of the C–H stretch of neat acetonitrile,[10] the C–H stretch of 1,1-d_2-ethanol,[13] and C≡N stretch of neat

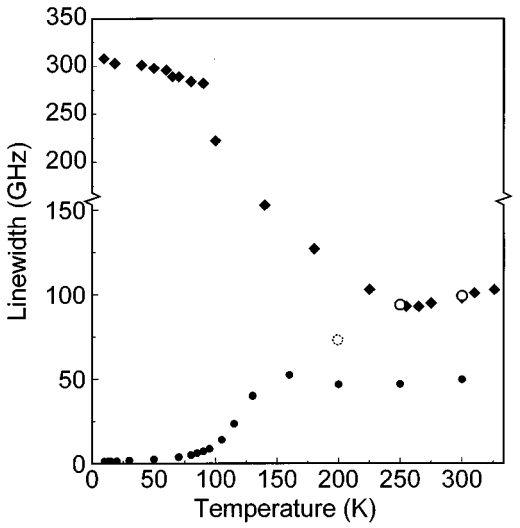

FIG. 7. Temperature dependence of the homogeneous and absorption linewidths for the T_{1u} mode of $W(CO)_6$ in 2-MP. The homogeneous linewidths (solid circles) are taken from Fig. 2 and the absorption linewidths (diamonds) are those taken from Fig. 3(c). The "echo" data at 250 and 300 K are actually free induction decays that match the observed absorption line (open circles), showing the spectra are homogeneously broadened. At 200 K (dotted circle), the homogeneous and inhomogeneous contributions to the absorption line are of equal magnitude. This point is only an interpolation between the 160 K and 250 K points. Below 200 K, the homogeneous linewidth is much narrower than the inhomogeneous width.

benzonitrile[12] using Raman echo experiments have determined that these vibrational bands are homogeneously broadened. Inhomogeneous broadening at room temperature has been observed with Raman echo experiments on the C–H stretch in $CH_3I/CDCl_3$ mixtures.[11] The source of inhomogeneity in this case is due to concentration fluctuations of the two types of molecules within the first solvation shell.

B. Total analysis of contributions to the homogeneous line shape in 2-MP

1. Transition to a homogeneously broadened line

The measured homogeneous vibrational linewidth obtained from infrared photon echo measurements (Fig. 2) assumed that the echo decays as Eq. (10b). This equation is valid in the inhomogeneous limit, when the width of the inhomogeneous distribution of homogeneous lines Δ far exceeds the homogeneous linewidth Γ. The inhomogeneous limit implies that a separation of time scales exists between the fast fluctuations of homogeneous dephasing and long time-scale inhomogeneous structural evolution.

Above 150 K, the homogeneous linewidth begins to approach the measured absorption linewidth, as illustrated in Fig. 7. Under these conditions, the time scale for the rephasing of the echo pulse is shortened by the polarization decay due to homogeneous dephasing. This causes the echo to rephase at times between τ and 2τ. Thus, the echo signal decays at a slower rate than the $4/T_2$ given by Eq. (10b).[54,55] In the limit that the absorption line is homogeneously broadened, a free induction decay (FID) will be observed along the echo phase matching direction. If the homogeneous line is a Lorentzian, then an exponential decay with a decay constant of $2/T_2$ will be observed.[55]

The data above 150 K reflect this transition to a homogeneously broadened line. If near room temperature the measured echo data are actually FIDs from a homogeneously broadened line, the decay constants $2/T_2$ yield a linewidth given by the open circles in Fig. 7. The FID linewidths match the measured absorption linewidths exactly, demonstrating that the line is homogeneously broadened for temperatures $\geqslant$250 K. Notice that the absorption linewidth, which narrows for temperatures up to 200 K actually broadens slightly for higher temperatures, in a manner that precisely follows the echo data. Without experimentally time resolving the rephasing of the echo pulse, it is not possible to determine from an echo experiment alone if the observable is a true echo decay, a FID, or an intermediate case. However, a comparison to the absorption spectrum provides a test. Since treating the point at 160 K as a FID still results in a linewidth that is narrower than the absorption line, this point corresponds to a true photon echo. The point at 200 K represents the transition between a homogeneous and inhomogeneous absorption line shape, and is merely added as an interpolation.

2. Orientational relaxation and restricted orientational relaxation

Pump–probe studies of the population dynamics of the T_{1u} mode of $W(CO)_6$ in 2-MP have observed dynamics that contribute to the infrared absorption line shape.[15] In addition to pure dephasing, population relaxation and orientational relaxation of the initially excited dipole contribute to the homogeneous linewidth. The contributions to the homogeneous vibrational linewidth measured with the photon echo are given by Eqs. (4) and (5). Using previous pump–probe measurements of the orientational diffusion constant D_{or} and the population relaxation time T_1,[15] the contribution due to pure dephasing can be determined from the homogeneous linewidth.

Although the viscosity of 2-MP changes over 14 orders of magnitude between 300 and 80 K, orientational relaxation slows by less than one order of magnitude over this range.[15] The orientational relaxation is distinctly nonhydrodynamic. This is because the orientational relaxation is not due to physical rotation of the molecule, but rather an evolution of the nature of the initially excited superposition of the triply degenerate T_{1u} modes.[15] The initial excitation creates a superposition state of the three basis states taken to be asymmetric CO stretches along the three molecular axes. The amplitudes, or coefficients, of a given basis state in the initial superposition is given by the projection of the E-field onto the direction of the basis state. Fluctuations of the environment cause time evolution of these coefficients, resulting in orientational randomization of the initially excited ensemble of dipoles. This reorientation is well described as isotropic Brownian orientational diffusion of the dipole.[15] Pump–probe experiments allow the determination of the orientational diffusion constant in Eq. (5).

Although this describes the high temperature ($T>125$ K) behavior of the 2-MP system, at lower temperatures, full orientational relaxation does not occur. Rather, the orientation is restricted and can be interpreted as diffusion within a

cone of semiangle θ_0.[56–58] Although the interpretation of pump–probe data within this model is well understood,[15] no such theory exists for the analysis of photon echo experiments. The influence of restricted orientational relaxation on the echo data is not dramatic at most temperatures. However, near the glass transition, echo decays are distinctly nonexponential, leading to non-Lorentzian homogeneous line shapes. In Appendix B, we discuss the details of a treatment of restricted orientational relaxation for the photon echo experiment. As demonstrated in the following section, this nonexponentiality does not invalidate the discussion of the previous sections in terms of exponential fits since the deviations from Lorentzian line shapes are small.

As with the treatment of complete orientational relaxation, we consider the case where the orientational and vibrational degrees of freedom are decoupled, so that the dipole correlation function can be written as Eq. (2). In the limit of small cone angles ($\theta_0<60°$), the two-time orientational correlation function decays as

$$C_{\mathrm{OR}}(t_i)=(S_1)^2+(1-(S_1)^2)c^1_{\nu^1_1}(t_i), \tag{12}$$

where $S_1=(1+\cos\theta_0)/2$. The exponential term $c^m_{\nu^m_n}$ is defined as in Eq. (6), but for the noninteger factors ν^m_n. The factors ν^m_n are functions of θ_0, and are discussed in Appendix B. In the limit of complete orientational relaxation, $S_1=0$ and $\nu^m_n\rightarrow l$, and the expression for complete orientational relaxation is obtained. Equation (12) shows the primary feature of restricted orientational relaxation: the correlation function decays to a nonzero value related to the degree of restriction, i.e., the cone angle. For the two-time restricted orientational correlation function, the long time value ($t=\infty$) is given by $\langle\mu\rangle^2=S_1^2$ which is the constant offset in Eq. (12). For the four-time correlation function, the long time offset is $\langle\mu\rangle^4=S_1^4$.

If, as with the complete orientational relaxation, the four-time correlation function can be described as the product of two two-time correlation functions, then the echo signal (see Appendix B) is given by

$$I(\tau)/I(0)=|C_V C_{\mathrm{OR}}|^2=\exp(-4\tau(1/T_2^*+1/2T_1))\times[(S_1)^2+(1-(S_1)^2)c^1_{\nu^1_1}(t_i)]^4. \tag{13}$$

In the limit that the cone angle grows to 180°, $S_1=0$ and $\nu^1_1\rightarrow l=1$, and the signal for complete orientational relaxation in Eq. (10a) is recovered. Likewise for the case when no orientational relaxation occurs at all, $\theta_0=0°$, and the exponential decay of the signal is due only to the vibrational terms. For intermediate cases, it is observed that the effect of restricted orientational relaxation on the echo signal decay is relaxation to an offset of (S_1),[8] the result predicted for the square of the four-time correlation function. This high order dependence demonstrates the sensitivity of the echo technique to restricted orientational relaxation. The offset $(S_1)^8$ allows the cone angle to be determined, and the cone angle determines ν^m_n for the fit of the orientational diffusion constant.

From Eq. (13) it is clear that when the dynamics of restricted orientational relaxation are faster than those for population relaxation and pure dephasing, the echo decay allows the orientational contribution to be separated from the other dynamics influencing the echo decay. Once the orientational dynamics have decayed, the residual decay is due only to the vibrational terms. A fit to the tail of the decay determines $(1/T_2^* + 1/2T_1)$ independently from the orientational dynamics. This is particularly useful in the small cone angle limit. As the cone angle shrinks, the orientational decay to $(S_1)^2$ becomes faster. This rapid orientational decay, followed by the exponential relaxation due to the vibrational term, is observed as a clear division of time scales in the decay.

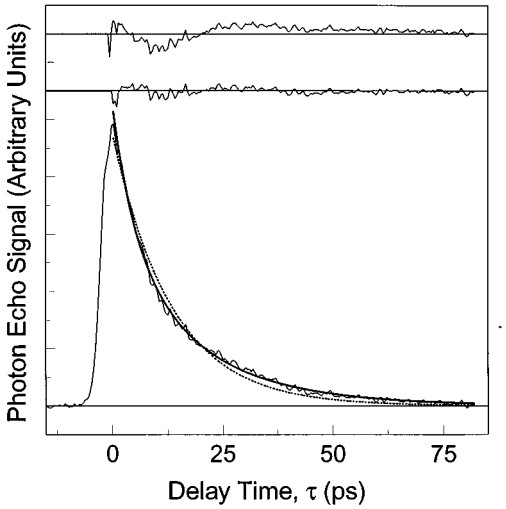

FIG. 8. Photon echo data, fits, and residuals for the T_{1u} mode of $W(CO)_6$ in 2-MP at 85 K. To demonstrate that the data are not exponential, two fits are shown: a single exponential fit (dashed line) and a fit to the model including restricted orientational relaxation (solid line) given by Eq. (13). The residuals for the exponential (top) and Eq. (13) (bottom) fits are given to allow comparison. The nonexponential echo decay means that the homogeneous line shape is not Lorentzian.

An example of a fit of Eq. (13) to echo data at 85 K is shown in Fig. 8 (solid line). Also shown is an exponential fit (dashed line) and the residuals of the fits. The data are clearly nonexponential, with an initial contribution due both to the vibrational and orientational dynamics, followed by a tail that will decay at a rate determined by the vibrational correlation function. The quality of the fit obtained with Eq. (13) is good for all temperatures. At low temperatures, it fits the fast but small amplitude restricted orientational decay component, which is observed as a small deviation from exponentiality. At intermediate temperatures, given the good signal-to-noise ratio, the deviations from exponential decays are pronounced, as in Fig. 8. At higher temperatures, when the cone angle approaches complete orientational relaxation, obtaining accurate values of the orientational parameters solely from the echo decay becomes difficult, since the rate of pure dephasing far exceeds the orientational contribution.

The functional form of Eq. (13) is correct, i.e., the restricted orientational relaxation will cause a decay to a nonzero value. It can be used to extract the time dependence of the orientational and vibrational contributions to homogeneous dephasing. However, there are clear indications that it is not quantitative. A quantitative relationship would permit

the cone angle and the orientational diffusion constant to be obtained from the decay constant and magnitude of the decay caused by restricted orientational relaxation. Analyzing the echo data with Eq. (13) does not yield the cone angles and diffusion constants obtained for this system from the analysis of the pump–probe experiments.[15] In the glass, the cone angles obtained from the echo data are consistently smaller by ~50% than the cone angles obtained from pump–probe data. The diffusion constants obtained from the echo data are equal within error bars to those derived from pump–probe data at low temperatures, but are anomalously high between 70 and 100 K.

Since the theoretical analysis used to analyze the pump–probe experiments is well defined,[15] the lack of agreement suggests uncertainty in the more complex problem of the theoretical description of the influence of restricted orientational relaxation on the echo signal. The separability of the four-time correlation function is based on assuming a Markovian process. In general, higher-order correlation functions can be expressed in their two-time equivalents if the probability function for a given time interval is independent of the history of previous processes.[59] This is not the case for restricted orientational relaxation. The true form needs to be determined using the full four-time correlation function. For complete orientational relaxation, which occurs at the higher temperatures, the decay is exponential, and the four-time correlation function can be factored. The derivation of the echo decay for complete orientational relaxation is given in Appendix A and for restricted orientational relaxation is given in Appendix B.

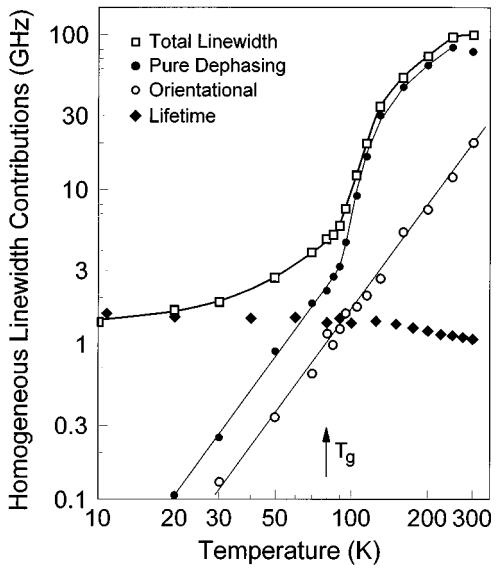

FIG. 9. Log–log plot of the dynamic contributions to the homogeneous vibrational linewidth of the T_{1u} mode of $W(CO)_6$ in 2-MP. The total linewidth—squares; lifetime contribution—diamonds; pure dephasing contribution—solid circles; orientational contribution—open circles. The lifetime dominates the homogeneous linewidth at the lowest temperatures and is only mildly temperature dependent. At high temperatures, pure dephasing dominates the homogeneous linewidth. Orientational relaxation never dominates but makes significant contributions to the linewidth at intermediate temperatures. The total homogeneous linewidths were determined directly from the dynamic variables T_1, T_2^*, D_{or}, and θ_0, and are identical to the data in Fig. 7 within experimental error. Lifetime contributions are taken from Fig. 3. The orientational contribution, shown with a $T^{2.2}$ power law line, is continuous over all temperatures. The line through the pure dephasing data is a fit to Eq. (16). Error bars on the total linewidth, lifetime, and pure dephasing are approximately the size of the symbols at most temperatures. The orientational error bars vary from the size of the symbols at high temperature to ±50% at 30 K.

3. Contributions to the homogeneous vibrational line shape

By combining the photon echo and pump–probe data, all of the dynamics that contribute to the homogeneous line shape are known. At higher temperatures, pump–probe experiments demonstrate that there is full orientational relaxation and can be used to measure the orientational diffusion constant.[15] Full orientational relaxation results in an exponential decay of the correlation function, and thus a Lorentzian contribution to the line shape. Therefore, all contributions to the echo decay are exponential, and the homogeneous line shape is Lorentzian with width given by Eqs. (4) and (5). The homogeneous infrared line shape in the absence of inhomogeneous broadening is given by Eq. (1).

As described in Appendix B, the two-time correlation function for restricted orientational relaxation has been given by Wang and Pecora.[57] The small cone angle result is Eq. (12). The photon echo data at long times give $1/T_2^* + 1/2T_1$, and pump–probe experiments give T_1, D_{or}, and θ_0.[15] Since these are the dynamic parameters that contribute to the line shape, the homogeneous line shape can be determined from Eq. (1), where

$$\langle \mu(t)\mu^*(0)\rangle = \exp(-t(1/T_2^* + 1/2T_1)) \times [(S_1)^2 + (1-(S_1)^2)c^1_{\nu_1^1}(t)] \qquad (14)$$

in the small cone angle limit. For data below 125 K, Eq. (14) applies,[15] and the homogeneous line shape is given by the sum of two Lorentzians.

As seen from Eq. (14), one of the Lorentzian contributions to the line shape is due purely to the vibrational relaxation terms $(1/T_2^* + 1/2T_1)$, and the other is a convolution of the orientational and vibrational terms. Combining the photon echo and pump–probe results allows the individual dynamic contributions to the total linewidth to be quantified. At temperatures >125 K, the line is Lorentzian with contributions to the linewidth (FWHM) described by Eq. (4). Using the T_1 and D_{or} measured with the pump–probe experiment, the contribution of pure dephasing to the line can be obtained. At lower temperatures, the vibrational line is non-Lorentzian, but all dynamics contribute to the FWHM linewidth based on their amplitudes. Using the linewidth from line shapes obtained from Eq. (14), T_1 from the pump–probe experiments, and T_2^* obtained from the echo data, the orientational contribution can be determined by difference.

In Fig. 9, the various contributions to the homogeneous linewidths are given. Although the manner of analysis of the dynamics changes at 125 K, the temperature dependence of each of the contributions is continuous. The total linewidth, obtained directly from the dynamic variables T_1, T_2^*, D_{or},

and θ_0, match the numbers from an exponential fit to the echo data in Fig. 2 almost exactly. There is only a slight deviation (<10%) for the temperatures between 80 and 95 K. The single exponential fit, although inadequate for determining the line shape in regions of restricted orientational relaxation provides a very good number for the FWHM linewidth. This conclusion provides the basis for the discussion of the temperature dependence of the homogeneous linewidths of the other liquids given in Secs. IV and V A.

Figure 9 displays the decomposition of the temperature dependence of the homogeneous vibrational linewidth into its three dynamic components. At low temperatures, the lifetime is the dominant contribution. At high temperatures, pure dephasing is the dominant contribution. Only at intermediate temperatures does orientational relaxation make a substantial contribution. The linewidth contribution from lifetime broadening remains significant until ~50 K. The mild temperature dependence of T_1 shows that it is adequate to subtract a constant, Γ_0, for the lifetime contribution in Eq. (11). Above 50 K, the contributions to the linewidth from pure dephasing and orientational relaxation dominate. By 100 K, the pure dephasing is a substantially larger contribution than either the lifetime or the orientational relaxation, and the overwhelmingly dominant component of the homogeneous linewidth above ~150 K.

At low temperature, where the contributions from pure dephasing and orientational relaxation are negligible, the contribution to the linewidth from the lifetime (from pump–probe data) and the linewidth determined from the decay of the echo are equal within error. This is the expected low temperature limit for the homogeneous vibrational linewidth where processes caused by thermal fluctuations disappear, and only lifetime broadening is possible.[31,32]

From low temperature to slightly above T_g, both pure dephasing and orientational relaxation have power law temperature dependences. The earlier discussion of the combined dynamics in 2-MP and the other two solvents showed a T^2 temperature dependence when the lifetime contribution was taken out. Here, the contributions from each mechanism are shown to follow the same T^2 power law behavior in the glass. Thus the total temperature dependence, excluding T_1, is T^2, as shown in Figs. 5 and 6. In addition, the power law observed for the orientational relaxation in the glass is observed to continue into the liquid. In Fig. 9, a power law fit of $\alpha=2.2\pm0.2$ is shown. The orientational dynamics are independent of the glass transition and distinctly nonhydrodynamic. The orientational relaxation does not have the temperature dependence of the viscosity. This is consistent with the results of pump–probe experiments.[15]

In Fig. 9 it is seen that there is a rapid increase in pure dephasing above the glass transition temperature. This implies the onset of an additional mechanism operating on the appropriate time scale to cause pure dephasing and linked to the glass-to-liquid transition. The onset of dynamic processes near the glass transition is often described with a Vogel–Tammann–Fulcher equation[50,60,61]

$$\tau=\tau_0\ \exp(B/(T-T_0)). \tag{15}$$

This equation describes a process characterized by a time, τ, with a temperature-dependent activation barrier that diverges at a temperature, T_0, below the nominal glass transition temperature [$\eta(T_g)=10^{13}$ poise]. T_0 can be linked thermodynamically to an ''ideal'' glass transition temperature that would be measured with an ergodic observable.[50] This equation describes the temperature dependence of the viscosity of 2-MP well, and gives $T_0=59$ K.

If the Vogel–Tammann–Fulcher (VTF) equation applies to pure dephasing near and above the glass transition, then the full temperature dependence is given by the sum of the low temperature power law and a VTF term:

$$\Gamma^*(T)=A_1T^{\alpha}+A_2\ \exp(-B/(T-T_0^*)). \tag{16}$$

A fit to Eq. (16) for all temperatures below 300 K is shown as the line through the pure dephasing data in Fig. 9. The fit describes the entire temperature dependence exceedingly well, but yields a reference temperature of $T_0^*=80$ K. This reference temperature matches the laboratory glass transition temperature T_g exactly not the ideal glass transition temperature T_0. We can thus infer that the onset of the dynamics that cause the rapid increase in homogeneous dephasing in 2-MP is closely linked with the onset of structural processes near the laboratory glass transition temperature. This may be a manifestation of the short time scale of the measurement and a reflection of the nonergodicity of the system.

The temperature dependence given by Eq. (16) does not describe the decrease in the pure dephasing linewidth observed for the 300 K point. This may be explained by motional narrowing of the line,[35] which is consistent with the observed transition to a homogeneously broadened absorption line at 250 K.

4. Relationship to theories of pure dephasing in liquids

The data presented here can be compared with the predications of a number of theories for the temperature dependence of vibrational dephasing in liquids.[4,16,17,33] A number of the theories for vibrational pure dephasing in liquids are based on vibrational–translational coupling and collision-induced frequency perturbations and yield results that are related to viscosity. Lynden-Bell relates vibrational dephasing to translational diffusion within the liquid potential and obtains a temperature dependence $1/T_2^* \propto \rho\eta/T$.[62] The isolated binary collision (IBC) model of Fischer and Laubereau[63] relates the linewidth to dephasing collision probability yielding $1/T_2^* \propto \eta T/\rho$. The hydrodynamic model of Oxtoby[64] obtains results similar to the IBC model, $1/T_2^* \propto \eta T$. In these expressions, the temperature dependence of the viscosity, η, is the dominant factor.

None of these theories can describe the data in this study. Although the viscosity in liquid 2-MP increases by approximately 14 orders of magnitude between 80 and 300 K, the rate of pure dephasing changes by less than 2 orders of magnitude. The problem may be that the viscosity does not form an adequate approximation for the collision frequency,[4] or that an explicit mechanism for dephasing in a particular system may be necessary to explain the temperature dependence.

Schweizer and Chandler have calculated the vibrational dephasing due to fast interactions with the repulsive wall of the potential based on an Enskog collision time.[18] This theory predicts a temperature dependence of $1/T_2^* \propto \rho T^{3/2} g(\sigma)$, where $g(\sigma)$, the contact value of the radial distribution function for a spherical solvent with diameter σ, may be mildly temperature dependent. This temperature dependence comes much closer to describing the pure dephasing of $W(CO)_6$ in 2-MP between 130 and 275 K, but does not reflect the rapid increase in the viscous, supercooled liquid between 80 and 130 K.

A description of vibrational dephasing above the glass transition that is valid for viscous fluids is clearly necessary. Such a theory might benefit from some of the approaches to amorphous media that are used for the theories of high temperature dephasing in glasses. The data presented here have demonstrated the existence of continuous T^2 behavior through the glass transition with the rapid onset of an additional or modified dephasing process above the glass transition at a temperature.

VI. CONCLUDING REMARKS

The infrared photon echo and pump–probe experiments presented above have allowed a complete characterization of the temperature dependence of the infrared vibrational homogeneous line shape of the T_{1u} CO stretching mode of $W(CO)_6$ in three molecular glass forming liquids. This work has quantified the degree of inhomogeneous broadening, the dynamic contributions to the homogeneous vibrational line shape, and the temperature dependences of these quantities. Results are followed from the nonequilibrium low temperature glass, through the glass transition and supercooled liquid, to the equilibrium room temperature liquid.

To completely characterize the infrared line shape, a combination of experimental methods is necessary to elucidate each of the dynamic and static contributions to the line. Picosecond infrared photon echo experiments were used to measure the homogeneous line shape and remove inhomogeneity. Infrared pump–probe experiments were used to measure the vibrational lifetime and orientational relaxation. The total vibrational line shape was determined by absorption spectroscopy. Together, these experiments yield a complete characterization of the dynamics that make up the homogeneous line, and the extent of inhomogeneity of the infrared absorption line.

Several key finding of this study are worth stating. At low temperatures, the homogeneous linewidth is determined by the vibrational lifetime. From 10 K to slightly above the glass transition, a T^2 temperature dependence for the vibrational pure dephasing is observed in all three solvents, indicating dephasing through a two-phonon Raman scattering process. In the glass and supercooled liquid, orientational relaxation is incomplete, leading to nonexponential echo decays and non-Lorentzian homogeneous line shapes. However, the orientational relaxation contribution to the total homogeneous line shape is never dominant, and the deviations from Lorentzian are not great. In the liquid, above ~125 K, orientational relaxation is complete and, therefore, the homogeneous line shape is Lorentzian. The role of orientational relaxation and the effect of restricted orientational relaxation on photon echo observables has been examined in some detail theoretically in the Appendices. While the dynamics are universal in the three glasses studied, they differ in the liquids for temperatures above $\sim 1.2 T_g$. The homogeneous dephasing in the liquids are independent of their hydrodynamic characteristics, having a much milder temperature dependence than the viscosity. At room temperature, the vibrational line is homogeneous in the solvent 2-methylpentane but substantially inhomogeneous in dibutylphthalate.

The homogeneous line shape in the 2-methylpentane solvent was decomposed into its three components, pure dephasing, orientational relaxation, and vibrational lifetime, over the entire temperature range of 10–300 K. The vibrational lifetime has a very mild temperature dependence and dominates the linewidth at low temperature. The orientational relaxation contribution has a T^2 temperature dependence over the entire range with no discontinuity near the glass transition temperature. Its contribution, while significant in some temperature ranges, never dominates the linewidth. The temperature dependence of the pure dephasing contribution to the linewidth is described by a T^2 power law in the glass but becomes much steeper above the glass transition. Its temperature dependence can be fit well to the sum of the power law and a Vogel–Tammann–Fulcher equation. However, the Vogel–Tammann–Fulcher divergence temperature is T_g rather than the ''ideal'' glass transition temperature 20 K below T_g.

While the study presented here gives detailed results from three solvents, it examines only one mode of one molecule. Clearly the time-domain methods that have been employed here to obtain a complete determination of the temperature-dependent vibrational dynamics need to be applied to other systems. Vibrational photon echoes combined with pump–probe experiments will allow accurate decomposition of vibrational line shapes that are convolutions of multiple dynamic and static contributions acting on widely variable time scales.

ACKNOWLEDGMENTS

The authors gratefully acknowledge David Zimdars, Dr. Randy Urdahl, Dr. Bernd Sauter, Rick Francis, and Dr. Alfred Kwok who contributed to the acquisition of the data discussed in this paper. The authors thank Professor Alan Schwettman and Professor Todd Smith of the Department of Physics at Stanford University and their groups for the opportunity to use the Stanford Free Electron Laser. We also thank Dr. Camilla Ferrante for many helpful discussions. This work was supported by the National Science Foundation (DMR93-22504), the Office of Naval Research (N00014-92-J-1227), the Medical Free Electron Laser Program (N00014-91-C-0170), and the Air Force Office of Scientific Research (F49620-94-1-0141).

APPENDIX A: CONTRIBUTION OF ORIENTATIONAL RELAXATION TO THE THIRD-ORDER POLARIZABILITY

Here we describe the effect of orientational relaxation on the stimulated photon echo response function for an inhomogeneously broadened line comprised of motionally narrowed homogeneous lines, i.e., the Bloch limit. The photon echo is the limiting case of the stimulated echo in which the second and third pulses are simultaneous. Generally, the third-order material response[39,65] is written for isotropic media, or unpolarized light. A proper treatment of orientational anisotropy in time-domain third-order (four-wave mixing) experiments requires a tensorial nonlinear response function formalism. This formalism has been presented by Cho *et al.*,[66] but only derived for pump–probe experiments.

The density matrix description of resonant third-order nonlinear experiments in terms of four-time correlation functions has been given by others,[6,39–42] and is not discussed here. The experimental four-time correlation functions are given by the third-order response function $\mathbf{R}$, and are related to the signal through the third-order polarization $\mathbf{P}$[39,40,41,66]

$$\begin{aligned}\mathbf{P}_\eta(\mathbf{k},t)=(-i^3)\int_0^\infty dt_3\int_0^\infty dt_2\int_0^\infty dt_1\mathbf{R}_{\eta\alpha\beta\gamma}(t_1,t_2,t_3)\\ \times\exp(i(\omega_1+\omega_2+\omega_3)t_3+i(\omega_1+\omega_2)t_2\\ +i\omega_1 t_1)E_{3\alpha}(t-t_3)E_{2\beta}(t-t_3-t_2)\\ \times E_{1\gamma}(t-t_3-t_2-t_1).\end{aligned}\tag{A1}$$

Here $\mathbf{R}_{\eta\alpha\beta\gamma}(t_1,t_2,t_3)$ is the third-order tensorial nonlinear response function. This equation describes the signal generated at time t with wave vector $\mathbf{k}$ and polarization component η, due to three input pulses E_1, E_2, and E_3 with polarization components γ, β, and α. In Eq. (A1), t_1 and t_2 refer to the time intervals between interactions with the fields E_1, E_2, and E_3; t_3 is the time interval between E_3 and the observation time t.[39]

To greatly simplify this problem, it is assumed that the orientational motion is separable from the conventional isotropic response, i.e., the vibrational and orientational motions are not coupled in the system. Further, the orientational behavior of the excited coherent state is assumed to be similar to that of the ground state. These assumptions (discussed below) allow us to write

$$\mathbf{R}_{\eta\alpha\beta\gamma}(t_1,t_2,t_3)=R_{\mathrm{OR}}(t_1,t_2,t_3)R_V(t_1,t_2,t_3),\tag{A2}$$

where R_{OR} is the orientational contribution to the response function, and R_V is the conventional isotropic vibrational response function. R_{OR} contains only the time-dependent orientational information and the dependence on the input field polarizations, α, β, and γ, while the remaining dipole-coupling terms are contained in R_V.

To describe the contribution of orientational diffusion to the third-order response function in the Bloch limit, we consider the case of three delta function pulses incident along the x laboratory axis, with parallel linear z axis polarizations. The generalization to any polarization is straightforward. We consider an ensemble of spherical rotors with nondegenerate dipole transitions with orientations Ω. We write Ω to refer to the spherical coordinates (θ,ϕ), with $\int d\Omega=\int_0^{2\pi}d\phi\int_0^{\pi}\sin\theta d\theta$. The classical orientational diffusion of such a dipole is well known.[36,37] Orientational diffusion is described by $G(\Omega,t|\Omega_0)$, the probability evolution Green's function that satisfies the orientational diffusion equation, which gives the probability that if μ has direction Ω_0 at time $t=0$, then it will have direction Ω at time t. $G(\Omega,t|\Omega_0)$ is a well-known function that is given by an expansion in spherical harmonics[67]

$$G(\Omega_i,t_i|\Omega_0)=\sum_{l=0}^{\infty}\sum_{m=-l}^{l}c_l^m(t_i)[Y_l^m(\Omega_0)]^*Y_l^m(\Omega_i),\tag{A3}$$

where the expansion coefficients c_1^m are given by Eq. (6). Evaluation of probability functions for linear spectroscopies are greatly simplified by the orthogonality of spherical harmonics. Such correlation functions can generally be expressed in the form of $\langle P_l(\hat{\mu}(t)\cdot\hat{\mu}(0))\rangle$, where P_l is the lth order Legendre polynomial ($m=0$), and can be expressed in terms of the expansion coefficients [Eq. (A6)]. In particular, it can be shown that[67]

$$\langle P_1(\hat{\mu}(t)\cdot\hat{\mu}(0))\rangle=c_1(t),\tag{A4a}$$

$$\langle P_2(\hat{\mu}(t)\cdot\hat{\mu}(0))\rangle=c_2(t).\tag{A4b}$$

The first equality is of importance in dielectric relaxation measurements and infrared line shapes, while the second is used for Raman scattering, light scattering, pump–probe experiments, and fluorescence depolarization.[3,34]

For the stimulated echo, the orientational contribution to the third-order polarizability is given by a four-time joint probability function[66]

$$\begin{aligned}R_{\mathrm{OR}}(t_3,t_2,t_1)=\int d\Omega_3\int d\Omega_2\int d\Omega_1\int d\Omega_0(\hat{\mu}_3\cdot\hat{\epsilon}_\eta)\\ \times G(\Omega_3,t_3|\Omega_2)(\hat{\mu}_2\cdot\hat{\epsilon}_\alpha)G(\Omega_2,t_2|\Omega_1)\\ \times(\hat{\mu}_1\cdot\hat{\epsilon}_\beta)G(\Omega_1,t_1|\Omega_0)(\hat{\mu}_0\cdot\hat{\epsilon}_\gamma)P(\Omega_0),\end{aligned}\tag{A5}$$

where $P(\Omega_0)$ is the initial dipole distribution and $(\hat{\mu}_i\cdot\hat{\epsilon}_j)$ represents the interaction of the field with the distribution of dipoles at time t_i. For an initially isotropic sample $P(\Omega_0)=1/4\pi$. Here we consider all incident pulses polarized parallel along the z axis, so that

$$(\hat{\mu}_i\cdot\hat{\epsilon}_j)=\cos\theta_i=P_1(\cos\theta_i).\tag{A6}$$

Substitution of Eqs. (A3) and (A6) into Eq. (A5), with parallel detection polarization, yields

$$R_{\mathrm{OR}}(t_1,t_2,t_3)=\tfrac{1}{9}c_1(t_1)[1+\tfrac{4}{5}c_2(t_2)]c_1(t_3).\tag{A7}$$

This result shows that the polarization of the two pulse photon echo experiment decays with time exponentially as $\exp[-2D_{\mathrm{or}}t]$. Equation (A7) also reproduces all polarization dependence of all parallel polarized four-wave mixing experiments. For pump–probe and transient grating experiments, $t_1=t_3=0$, and the well-known expression for the parallel-probed orientational signal is obtained. The orientational component of the signal decays exponentially as $\exp[-6D_{\mathrm{or}}t]$ to a constant offset of 0.56. Notice that the four-time correlation function given by Eq. (A7) can be writ-

ten, using Eq. (A4), as the product of two-time correlation functions. The two-pulse photon echo signal ($t_2=0$) gives the orientational dynamics in terms of $\langle P_1(\hat{\mu}(t)\cdot\hat{\mu}(0))\rangle$, just as represented in the infrared line shape.

The vibrational contribution to the response function R_V has been evaluated for a number of models,[6,42,68] and is not discussed here. For the dephasing and relaxation of the vibrational modes studied here, the fast modulation (Bloch) limit applies, and the vibrational response function has been given as[11]

$$R_V(t_1,t_2,t_3)=\exp[-(t_1+t_3)/T_2^*]\times\exp[-(t_1+2t_2+t_3)/2T_1]\times\exp[-\Delta^2(t_3-t_1)^2/2]. \tag{A8}$$

Here any dipole operator terms that reflect the amplitude of the signal have been suppressed. The excitation fields span the inhomogeneous line, which is described by a Gaussian distribution of homogeneous packets, $G(\omega)$, with a standard deviation in time of Δ. Notice that in the Markovian limit, where $t_1=t_3$, the four-time vibrational response function can be factored into the product of three two-time correlation functions. Thus, the entire four-time correlation function in the Bloch limit can be expressed as two-time correlation functions.[38]

For delta-function pulses, $E_i(t-t')=\delta(t-t')$, the polarization is given by the response function. For the two-pulse photon echo, $t_1=t_3=\tau$, $t_2=0$, and $\Delta=0$, and the signal is calculated from

$$I(2k_2-k_1,\tau)\propto|P(2k_2-k_1,\tau)|^2. \tag{A9}$$

For R_{OR} and R_V given by Eqs. (A7) and (A8), respectively, the echo signal is given by Eq. (10). For an echo signal decay due only to rotational diffusion, the echo signal decays exponentially at rate of eight times the orientational diffusion constant. This is in contrast to the anisotropy decay in pump–probe or fluorescence depolarization experiments, which decay as $6D_{\mathrm{or}}$. Notice that for this Markovian limit, in which the correlation functions decay exponentially, the signal is proportional to $|\langle\boldsymbol{\mu}(\tau)\cdot\boldsymbol{\mu}^*(0)\rangle|^4$.

The derivation of the expressions used here for the effect of orientational relaxation is based on the assumption that it is uncorrelated with the vibrational dynamics of the dipole. This assumption is often invoked to simplify the description of rotational motion in complex systems.[34,38,66] This assumption may be considered if a separation of time scales exists for the dynamics of vibrational dephasing and orientational relaxation. The rapid fluctuations of the bath allow its interaction with the vibrational coherence to be considered as a Markovian process in the weak coupling limit. Further, the influence of these fast bath fluctuations on the motion of the dipole allow the orientational motion to be treated as Brownian diffusion.

These generalizations are different for the current case, when we consider that the orientational motion of the initially excited dipole is not due to the physical rotation of the molecule. In fact, the orientational relaxation occurs through the evolution of the initially excited superposition state of the T_{1u} mode.[15] This process is independent of the solvent viscosity, and occurs due to thermal fluctuations in the environment that cause the coefficients of the basis states to evolve. However, the observation that reorientational motion is linked to spectral diffusion in the line[15] allows us to decouple these dynamics from the pure dephasing. Spectral diffusion, observed for temperatures below 200 K, is the evolution of the homogeneous transition frequencies in an inhomogeneous line on a time scale longer then that of the homogeneous pure dephasing.

A further assumption in the description of the role of rotational diffusion on the echo experiment is that the rotational behavior of the evolving excited and ground vibrational states are similar. This allows the rotational characteristics to be treated as uniform, and as classical diffusion. This assumption would most likely not be valid for electronic spectroscopy, when the differing electronic configurations and change of size or shape of the electronic cloud could dramatically effect the rotational characteristics. For the case of ground electronic state vibrational spectroscopy on stretching modes, this is not unreasonable. Vibrational excitation leads to an increased root-mean-squared displacement of the oscillating dipole, but this should not alter the rotational characteristics greatly.

In this treatment of orientational relaxation of the vibrational line shape, all expressions have been written for a well-defined dipole transition direction. It has been assumed that the results derived above can be applied to the degenerate T_{1u} mode. The basis for this assumption is the influence of orientational relaxation on the pump–probe experiment. For parallel excitation, the pump–probe data show a zero-time orientational amplitude of 0.44, which yields a polarization anisotropy of $r(0)=0.4$, as predicted for the isotropic reorientation of a nondegenerate system. The applicability of the results to a degenerate system needs to be confirmed by a full theoretical calculation, which is very complex.

APPENDIX B: RESTRICTED ORIENTATIONAL RELAXATION

This section describes the influence of restricted orientational relaxation on the orientational correlation function C_{OR}, and its effect on the two pulse photon echo experiment. Instead of diffusion on the surface of a sphere, restricted orientational diffusion is often modeled as Brownian diffusion of the dipole within a cone of semiangle θ_0 centered about the z axis ($0°\leqslant\theta_0\leqslant180°$). In this discussion, we follow the treatment of two-time correlation functions for restricted orientation relaxation within a cone by Wang and Pecora.[57] As shown previously, the description of the infrared line shape requires a knowledge of $C_{\mathrm{OR}}=P_1\langle\hat{\mu}(t)\cdot\hat{\mu}(0)\rangle$. The treatment of restricted orientational relaxation for $P_2\langle\hat{\mu}(t)\cdot\hat{\mu}(0)\rangle$ has been given in a number of studies.[56,58,69,70]

In general, the two-time dipole correlation function for the orientational relaxation within a cone will decay to a nonzero value, $(S_l)^2$, which gives a measure for the extent of orientational relaxation.[69] The factor S_l, the generalized order parameter, satisfies the inequality $0\leqslant S_l\leqslant1$, where $S_l=0$ describes unrestricted reorientation, while $S_l=1$ is no orien-

tational motion. The value of $(S_l)^2$ can be determined from the relationship[69]

$$\lim_{t\to\infty}\langle A(0)B(t)\rangle=\langle A\rangle\langle B\rangle. \tag{B1}$$

For the two-time dipole correlation function $P_1\langle\hat{\mu}(t_i)\cdot\hat{\mu}(0)\rangle$, the decay should be to

$$\left[(2\pi(1-x_0))^{-1}\int d\Omega P_1(x_0)\right]^2=((1+x_0)/2)^2=(S_1)^2, \tag{B2}$$

where $x_0\equiv\cos\theta_0$. The factor $[2\pi(1-x_0)]^{-1}$ normalizes the expression to ensure a uniform distribution within the cone at $t=\infty$. The functional form of the decay of the correlation function to S_l^2 cannot be written in closed form, but can be approximated by a number of methods.[57,58,71] In the limit of small cone angles, the decay is well approximated by an exponential-with-offset of the form

$$C_{\mathrm{OR}}(t)=S_1^2+(1-S_1^2)\exp(-\kappa D_{\mathrm{or}}t), \tag{B3}$$

where κ is an proportionality constant that relates the effective decay time to the orientational diffusion constant. In the limit of complete orientational relaxation, $S_1=0$ and $\kappa=l(l+1)$, and Eq. (6) is recovered.

The probability evolution function $G(\Omega,t|\Omega_0)$ for the diffusion within a cone is given by an expansion in spherical harmonics of noninteger degree ν_n^m

$$G(\Omega_i,t_i\,\Omega_0)=(2\pi(1-x_0))^{-1}\sum_{n=1}^{\infty}\sum_{m=-\infty}^{\infty}c_{\nu_n^m}^m(t_i)\times[Y_{\nu_n^m}^m(\Omega_0)]^*Y_{\nu_n^m}^m(\Omega_i), \tag{B4}$$

where the expansion coefficients are given by

$$c_{\nu_n^m}^m(t_i)=\exp(-\nu_n^m(\nu_n^m+1)D_{\mathrm{or}}t_i). \tag{B5}$$

The parameter ν_n^m is a function of the cone angle, yet cannot be obtained in closed form as such. The calculation of ν_n^m from the diffusion equation and its relation to the cone angle has been outlined elsewhere.[57]

Wang and Pecora have calculated the two-time dipole correlation function $\langle\hat{\mu}(t)\cdot\hat{\mu}(0)\rangle$ for first and second degree spherical harmonics. These are given by an infinite sum of exponentials of the form[57]

$$\langle\hat{\mu}(t)\cdot\hat{\mu}(0)\rangle\propto\sum_{n=1}^{\infty}D_n^m c_{\nu_n^m}^m(t), \tag{B6}$$

where the cone angle determines the coefficients D_n^m and the factors ν_n^m. Dipole correlation functions can be approximated by truncating the sum in Eq. (B6). For first degree spherical harmonics, the dipole correlation function is well approximated for any cone angle by[57]

$$P_1\langle\hat{\mu}(t_i)\cdot\hat{\mu}(0)\rangle=D_1^0+D_2^0\exp(-\nu_2^0(\nu_2^0+1)D_{\mathrm{or}}t_i)+D_1^1\exp(-\nu_1^1(\nu_1^1+1)D_{\mathrm{or}}t_i). \tag{B7}$$

For small cone angles ($\theta_0<60°$), $D_2^0\approx0$ and the two-time dipole correlation function is observed to decay exponentially to a constant value D_1^0. In this limit, comparison to Eq. (B3) shows that $(S_1)^2=D_1^0$ and the exponential decay is given by $c_{\nu_1^1}^1(t_i)$. In this limit, the parameter ν_1^1 is well approximated by $\nu_1^1(\nu_1^1+1)=24/7\theta_0^2$. In the limit of complete orientational relaxation ($\theta_0=180°$), the parameters ν_1^1 and ν_2^0 converge toward $l=1$ and $D_1^0=0$, so that Eq. (6) is recovered. For purposes of fitting in this work, calculated values of ν_n^m as a function of θ_0 were fit to empirical functions.[72]

The four-time correlation function for restricted orientational relaxation will likewise decay to a constant offset given by

$$\langle P_1(x_0)\rangle^4=((1+x_0)/2)^4=(S_1)^4. \tag{B8}$$

The four-time correlation function for two-pulse photon echo experiments has been shown in Appendix A to be written in the Markovian limit as a product of two-time correlation functions. Thus, the four-time orientational correlation function for the photon echo experiment would be written as the product of two-time correlation functions

$$C_{\mathrm{OR}}(t_1,t_3)=P_1\langle\hat{\mu}(t_1)\cdot\hat{\mu}(0)\rangle P_1\langle\hat{\mu}(t_1+t_3)\cdot\hat{\mu}(t_1)\rangle. \tag{B9}$$

Within this description, the two-pulse echo signal in the small cone angle limit is described by Eq. (13). Notice Eq. (13) shows the correct limits by decaying to S_1^4. In the limit of complete orientational relaxation, $S_1=0$ and $\nu_1^1=l=1$, and the result given by Eq. (10) is obtained. For completely restricted orientational relaxation, $S_1=1$, and orientational diffusion does not contribute to the signal. In each of these limits, the Lorentzian line shape is obtained. The limitations of this descriptions are pointed out in Sec. V B 2.

[1] R. G. Gordon, J. Chem. Phys. **43**, 1307 (1965).
[2] R. G. Gordon, Adv. Magn. Reson. **3**, 1 (1968).
[3] B. J. Berne, in *Physical Chemistry: An Advanced Treatise*, edited by D. Henderson (Academic, New York, 1971), Vol. VIII B.
[4] J. Yarwood, Annu. Rep. Prog. Chem., Sec. C **76**, 99 (1979).
[5] W. G. Rothschild, *Dynamics of Molecular Liquids* (Wiley, New York, 1984).
[6] R. F. Loring and S. Mukamel, J. Chem. Phys. **83**, 2116 (1985).
[7] D. Zimdars, A. Tokmakoff, S. Chen, S. R. Greenfield, and M. D. Fayer, Phys. Rev. Lett. **70**, 2718 (1993).
[8] A. Tokmakoff, D. Zimdars, B. Sauter, R. S. Francis, A. S. Kwok, and M. D. Fayer, J. Chem. Phys. **101**, 1741 (1994).
[9] A. Tokmakoff, A. S. Kwok, R. S. Urdahl, R. S. Francis, and M. D. Fayer, Chem. Phys. Lett. **234**, 289 (1995).
[10] D. Vanden Bout, L. J. Muller, and M. Berg, Phys. Rev. Lett. **67**, 3700 (1991).
[11] L. J. Muller, D. Vanden Bout, and M. Berg, J. Chem. Phys. **99**, 810 (1993).
[12] R. Inaba, K. Tominaga, M. Tasumi, K. A. Nelson, and K. Yoshihara, Chem. Phys. Lett. **211**, 183 (1993).
[13] D. Vanden Bout, J. E. Freitas, and M. Berg, Chem. Phys. Lett. **229**, 87 (1994).
[14] L. R. Narasimhan, K. A. Littau, D. W. Pack, Y. S. Bai, A. Elschner, and M. D. Fayer, Chem. Rev. **90**, 439 (1990).
[15] A. Tokmakoff, R. S. Urdahl, D. Zimdars, A. S. Kwok, R. S. Francis, and M. D. Fayer, J. Chem. Phys. **102**, 3919 (1995).
[16] D. W. Oxtoby, Adv. Chem. Phys. **40**, 1 (1979).
[17] J. Chesnoy and G. M. Gale, Adv. Chem. Phys. **70**, 297 (1988).
[18] K. S. Schweizer and D. Chandler, J. Chem. Phys. **76**, 2296 (1982).
[19] R. M. Macfarlane and R. M. Shelby, J. Lumin. **36**, 179 (1987).
[20] W. E. Moerner, A. R. Chraplyvy, and A. J. Sievers, Phys. Rev. B **29**, 6694 (1984).
[21] M. Dubs and H. H. Guenthard, J. Mol. Struct. **60**, 311 (1980).
[22] S. P. Love and A. J. Seivers, J. Lumin. **45**, 58 (1990).
[23] H.-G. Cho and H. L. Strauss, J. Chem. Phys. **98**, 2774 (1993).

[24] M. Schrempel, W. Gellermann, and F. Luty, Phys. Rev. B **45**, 9590 (1992).
[25] A. Tokmakoff, B. Sauter, and M. D. Fayer, J. Chem. Phys. **100**, 9035 (1994).
[26] U. Happek, J. R. Engholm, and A. J. Seivers, Chem. Phys. Lett. **221**, 279 (1994).
[27] H. Graener, T. Loesch, and A. Laubereau, J. Chem. Phys. **93**, 5365 (1990).
[28] E. J. Heilweil, R. R. Cavanagh, and J. C. Stephenson, Chem. Phys. Lett. **134**, 181 (1987).
[29] E. J. Heilweil, M. P. Casassa, R. R. Cavanaugh, and J. C. Stephenson, Annu. Rev. Phys. Chem. **40**, 143 (1989).
[30] S. Califano, V. Schettino, and N. Neto, *Lattice Dynamics of Molecular Crystals* (Springer, Berlin, 1981).
[31] V. M. Kenkre, A. Tokmakoff, and M. D. Fayer, J. Chem. Phys. **101**, 10618 (1994).
[32] S. Velsko and R. M. Hochstrasser, J. Phys. Chem. **89**, 2240 (1985).
[33] D. W. Oxtoby, Annu. Rev. Phys. Chem. **32**, 77 (1981).
[34] B. J. Berne and R. Pecora, *Dynamic Light Scattering* (Krieger, Malabar, FL, 1990).
[35] R. Kubo, in *Fluctuation, Relaxation, and Resonance in Magnetic Systems*, edited by D. Ter Haar (Oliver and Boyd, London, 1962).
[36] P. Debye, *Polar Molecules* (Dover, New York, 1945).
[37] A. Carrington and A. D. McLachlan, *Introduction to Magnetic Resonance* (Harper and Row, New York, 1967).
[38] S. Bratos and J.-C. Leicknam, J. Chem. Phys. **101**, 4536 (1994).
[39] S. Mukamel and R. F. Loring, J. Opt. Soc. Am. B **3**, 595 (1986).
[40] Y. J. Yan and S. Mukamel, J. Chem. Phys. **89**, 5160 (1988).
[41] Y. J. Yan and S. Mukamel, J. Chem. Phys. **94**, 179 (1991).
[42] R. F. Loring and S. Mukamel, Chem. Phys. Lett. **114**, 426 (1985).
[43] P. W. Anderson, B. I. Halperin, and C. M. Varma, Philos. Mag. **25**, 1 (1972).
[44] W. A. Phillips, J. Low Temp. Phys. **7**, 351 (1972).
[45] D. L. Huber, J. Non-Cryst. Solids **51**, 241 (1982).
[46] J.-L. Barrat and M. L. Klein, Annu. Rev. Phys. Chem. **42**, 23 (1991).
[47] E. Roessler, Phys. Rev. Lett. **65**, 1595 (1990).
[48] U. Buchenau, C. Schönfeld, D. Richter, T. Kanaya, K. Kaji, and R. Wehrmann, Phys. Rev. Lett. **73**, 2344 (1994).
[49] N. J. Tao, G. Li, and H. Z. Cummins, Phys. Rev. Lett. **66**, 1334 (1991).
[50] C. A. Angell, J. Phys. Chem. Solids **49**, 863 (1988).
[51] 2-MP viscosity data was compiled from the following sources: A. C. Ling and J. E. Willard, J. Phys. Chem. **72**, 1918 (1968); H. Greenspan and E. Fischer, J. Phys. Chem. **69**, 2466 (1965); C. Alba, L. E. Busse, D. J. List, and C. A. Angell, J. Chem. Phys. **92**, 617 (1990).
[52] 2-MTHF viscosity data were compiled from the following sources: A. C. Ling and J. E. Willard, J. Phys. Chem. **72**, 1918 (1968); D. Nicholls, C. Sutphen, and M. Szwarc, J. Phys. Chem. **72**, 1021 (1968).
[53] DBP viscosity data were compiled from the following sources: A. C. Ling and J. E. Willard, J. Phys. Chem. **72**, 1918 (1968); A. J. Barlow, J. Lamb, and A. J. Matheson, Proc. R. Soc. London Ser. A **292**, 322 (1966).
[54] M. Cho and G. R. Fleming, J. Chem. Phys. **98**, 2848 (1993).
[55] T. Joo and A. C. Albrecht, Chem. Phys. **176**, 233 (1993).
[56] K. Kinosita, Jr., S. Kawato, and A. Ikegami, Biophys. J. **20**, 289 (1977).
[57] C. C. Wang and R. Pecora, J. Chem. Phys. **72**, 5333 (1980).
[58] G. Lipari and A. Szabo, Biophys. J. **30**, 489 (1980).
[59] D. A. McQuarrie, *Statistical Mechanics* (Harper and Row, New York, 1976).
[60] C. A. Angell, J. Phys. Chem. **86**, 3845 (1982).
[61] G. H. Fredrickson, Annu. Rev. Phys. Chem. **39**, 149 (1988).
[62] R. M. Lynden-Bell, Mol. Phys. **33**, 907 (1977).
[63] S. F. Fischer and A. Laubereau, Chem. Phys. Lett. **35**, 6 (1975).
[64] D. W. Oxtoby, J. Chem. Phys. **70**, 2605 (1979).
[65] S. Mukamel, Annu. Rev. Phys. Chem. **41**, 647 (1990).
[66] M. Cho, G. R. Fleming, and S. Mukamel, J. Chem. Phys. **98**, 5314 (1993).
[67] T. Tao, Biopolymers **8**, 609 (1969).
[68] Y. J. Yan and S. Mukamel, Phys. Rev. A **41**, 6485 (1990).
[69] G. Lipari and A. Szabo, J. Am. Chem. Soc. **104**, 4546 (1982).
[70] A. Szabo, J. Chem. Phys. **81**, 150 (1984).
[71] G. Lipari and A. Szabo, J. Chem. Phys. **75**, 2971 (1981).
[72] Using the results of Wang and Pecora, it can be shown that a relationship given by Lipari and Szabo (Ref. 58) describes the parameter ν_1^1 in the limit of small cone angles: $\nu_1^1(\nu_1^1+1)=24/7\theta_0^2$. An empirical relationship that gives ν_1^1 within 1% for $50°<\theta_0<150°$ is $\nu_1^1 = 10^{1.676}{\theta_0}^{-0.8334}$, where θ_0 is in degrees. For $\theta_0<170°$, $\nu_0^2 = 10^{2.496}{\theta_0}^{-1.122}$.